

RESEARCH ARTICLE | MARCH 04 2024

Identification of local structures in water from supercooled to ambient conditions ^{EP}

Special Collection: [Water: Molecular Origins of its Anomalies](#)

Riccardo Foffi  ; Francesco Sciortino  

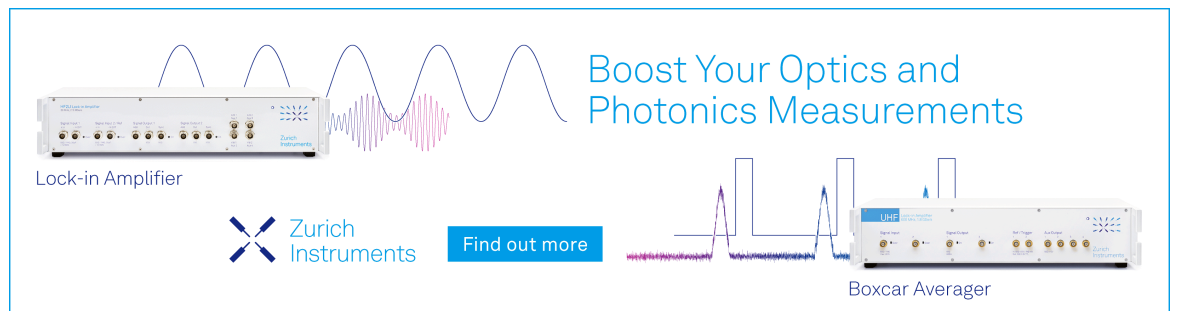
 Check for updates

J. Chem. Phys. 160, 094504 (2024)

<https://doi.org/10.1063/5.0188764>




CrossMark



Boost Your Optics and Photonics Measurements

Lock-in Amplifier

 Zurich Instruments

[Find out more](#)

Boxcar Averager

Identification of local structures in water from supercooled to ambient conditions

Cite as: J. Chem. Phys. 160, 094504 (2024); doi: 10.1063/5.0188764

Submitted: 23 November 2023 • Accepted: 9 February 2024 •

Published Online: 4 March 2024



View Online



Export Citation



CrossMark

Riccardo Foffi¹  and Francesco Sciortino^{2,a)} 

AFFILIATIONS

¹Department of Civil, Environmental and Geomatic Engineering, Institute for Environmental Engineering, ETH Zürich, Laura-Hezner-Weg 7, 8093 Zürich, Switzerland

²Dipartimento di Fisica, Sapienza Università di Roma, Piazzale Aldo Moro 5, I-00185 Rome, Italy

Note: This paper is part of the JCP Special Topic on Water: Molecular Origins of its Anomalies.

a) Author to whom correspondence should be addressed: francesco.sciortino@uniroma1.it

ABSTRACT

Studies of water thermodynamics have long been tied to the identification of two distinct families of local structures, whose competition could explain the origin of the many thermodynamic anomalies and the hypothesized liquid–liquid critical point in water. Despite the many successes and insights gained, the structural indicators proposed throughout the years were not able to unequivocally identify these two families over a wide range of conditions. We show that a recently introduced indicator, Ψ , which exploits information on the hydrogen bond network connectivity, can reliably identify these two distinct local environments over a wide range of thermodynamic conditions (188–300 K and 0–13 kbar) and that close to the liquid–liquid critical point, the spatial correlations of density fluctuations are identical to those of the Ψ indicator. Our results strongly support the idea that water thermodynamic properties arise from the competition between two distinct and identifiable local environments.

Published under an exclusive license by AIP Publishing. <https://doi.org/10.1063/5.0188764>

I. INTRODUCTION

Water is a liquid with fascinating physical properties.^{1–4} Differently from many other common compounds, the thermodynamic response functions of liquid water display a non-monotonic temperature and pressure dependence. For example, at ambient pressure, the compressibility has a minimum at 46 °C and a maximum at approximately –43 °C, and the density has a maximum at 4 °C.^{2,5} These non-monotonic behaviors are strongly suggestive of relevant structural changes taking place in the liquid state.

The peculiarities of water can be traced back to the strength and directionality of the hydrogen bond (HB) interaction and to the limited number of hydrogen bonds that a water molecule can form with its neighbors.^{6,7} Unlike other substances, water molecules can assume a variety of local structures, from the highly tetrahedral open configuration in which the water molecule participates in four linear hydrogen bonds to more distorted and denser local environments. The radial distribution function of the oxygen atoms indeed reveals the presence of interstitial molecules, located between the first and second tetrahedral shells.^{8,9} There is consensus that molecules in

“tetrahedral” configurations are characterized by low energy, local order, and low local density, while molecules at the other extreme are characterized by higher energies, higher disorder, and higher local density.^{10–12} If this large variety of configurations can be grouped into two families or if it reflects a continuum of geometries is still the object of controversy.^{13–15}

The idea of two families of different local environments is consistent with the hypothesized presence of a liquid–liquid critical point¹⁶ in supercooled states, the end point of a line of liquid–liquid first order transitions. Such a critical point, originally discovered in the ST2 water model,¹⁶ has recently been confirmed with accurate free-energy calculations in several high-quality classical potentials (TIP4P/2005, TIP4P/Ice,¹⁷ WAIL¹⁸), significantly strengthening the possibility that such an unconventional thermodynamic scenario is representative of real water. Neural network potentials based on quantum mechanics calculations¹⁹ and path-integral simulations²⁰ also support the presence of such a liquid–liquid critical point. Several experiments also support the liquid–liquid critical point scenario.^{5,21,22} In particular, recent x-ray scattering experiments probing sub-microsecond timescales to observe the relaxation of

the metastable liquid before nucleation have provided evidence of a transition between two different structures^{23,24} in deep supercooled states.

The presence of a critical point requires competition between two different local structures and a free-energy gain when local structures of the same type cluster in space. Several studies have shown that a simple two-state description of free-energy,^{10–12,25–29} in which the entropic term of mixing two different local structures (differing in energy, entropy, and density) is complemented by a clustering contribution, is able to describe the equation of states of several numerically studied models and to reproduce the equation of states of water better than any other previously proposed expression.³⁰

Numerical simulations have been thoroughly scrutinized, searching for quantities that could detect the two families of molecular structures.^{25,31–37} Unfortunately, most proposed indicators (but see for exceptions Refs. 25, 35, and 36), while based on strong physical intuitions, have typically resulted in wide distributions—which in some cases can be represented by the superposition of two distributions with relative weights changing with pressure and/or temperature. A clear indication of well separated two-state behavior (a distribution function with two well resolved peaks) has remained elusive. The ongoing attempt to include longer-range information in the definition of the structural indicators,^{38–41} despite its sound physical expectation, has not drastically improved the classification.

In an attempt to better characterize the features of the radial distribution function $g(r)$, we have recently developed^{42,43} an analysis connecting the physical distance between two molecules with their chemical distance, measured as the (smallest) number of hydrogen bonds that need to be crossed on going from one molecule to the other. All structural features appearing in $g(r)$ were thus associated with specific bonding geometries. In particular, the interstitial molecules, the ones populating the region around 3.5 Å between the first and second peak of the $g(r)$, have been associated with molecules with a chemical distance larger or equal to four. We have also found that a molecular order parameter (that we named Ψ_i), defined for each molecule i as the smallest distance in real space among all molecules with chemical distance four, has, close to the critical point, a well-defined bimodal distribution function. Tetrahedral, low-density local structures were found to be characterized by large values of Ψ_i (~ 6.5 Å), while high-density local structures favor shorter distances (~ 3.5 Å). Even more, at pressures close to the critical point, the average over all molecules in the system $\langle \Psi_i \rangle$ fluctuates exactly as the density,⁴⁴ confirming that $\langle \Psi_i \rangle$ could very well be chosen as the order parameter of the liquid–liquid transition.

In this article, we extend this analysis to a wide range of temperatures (from 180 to 300 K) and pressures (from 1 to 2500 bars) to quantify the temperature and pressure dependence of this indicator. At the lowest temperature, we extend the analysis to the very high density region (up to pressures of 13 kbar), presenting an interpretation of the very-high-density amorphous (VHDA) glass as the limiting structure composed of $\Psi_i \sim 3.5$ Å molecules.

II. METHODS

Most of the trajectories analyzed in this article have been previously generated^{42,43} using GROMACS 5.1.4⁴⁵ in the NPT ensemble

(Nosé–Hoover thermostat and Parrinello–Rahman barostat) and reproduce the dynamics of a system of 1000 rigid water molecules interacting via the TIP4P/Ice model.⁴⁶ To suppress thermal vibrations that are known to blur structural properties and hydrogen bond identification, we have calculated the inherent structures (IS),⁴⁷ the local potential energy minima, via a constant volume steepest descent path starting from equilibrated configurations. As previously performed,^{42,43} we find the IS using the steepest descent algorithm in GROMACS. The reproducibility of our MD simulations was tested against other TIP4P/Ice results recently reported by Lupi *et al.*⁴⁸ and Espinosa *et al.*⁴⁹ (see the supplementary material).

The presence of a hydrogen bond between two molecules is detected via the Luzar–Chandler geometric criterion.⁵⁰ In short, two molecules are hydrogen-bonded if the H–O–H angle is smaller than 30° and the oxygen–oxygen distance is smaller than 3.5 Å. When applied to IS, this criterion can properly identify the hydrogen bonds in the system over an extremely wide range of temperatures and pressures.⁴³

To evaluate the Ψ structural indicator, the chemical distance D between any pair of molecules i and j is calculated by counting the minimum number of hydrogen bonds that need to be traveled to move along the HB network from site i to site j . As we will show, the resulting Ψ histograms can be, for convenience, represented as a binary mixture of Burr type XII distributions.⁵¹

We also analyze new simulations of a system of 250 000 water molecules in the NVT ensemble at density 1.015 g/cm³ and $T = 191$ K. This state point, on the critical isochore, is quite close to the critical point such that density fluctuations at small wavevectors can be observed and correlated with the fluctuations of $\langle \Psi \rangle$.

III. RESULTS AND DISCUSSION

It is well established that, as water is exposed to increasing pressures, the oxygen–oxygen radial distribution function shows an increasing signal at separations around 3.5 Å, a distance that lies between the peaks of the first (2.8 Å) and second (4.5 Å) spatial shells of the liquid at ambient conditions.^{8,9} This feature, which signals a progressive distortion of the open tetrahedral geometry, has been well characterized over a broad range of conditions and becomes particularly evident in the amorphous ices when, upon crossing from high-density amorphous (HDA) to VHDA, an initially minor signal in this “interstitial” region transforms into a dominant peak, highlighting a drastic restructuring of the H-bond network.^{43,52} Interestingly, this interstitial population has been shown to arise from molecules that are at a chemical distance of four (or more) from the central one.⁴² It is important to stress that most of these interstitial molecules are still involved in four hydrogen bonds, albeit more distorted on average than in the open tetrahedral environment, and therefore, they cannot be directly associated with coordination defects (cf. three or five coordinated molecules) in the HB network, although some correlation exists.^{40,42} In previous work,⁴² we have shown that the distribution of real space distances between molecules at a chemical distance of four displays a clear separation between a group of molecules located around 3.5 Å and another group with distances of ≈ 8 Å. This significant separation in real space (3.5 vs 8.0 Å) has been exploited to build, in Ref. 44, a molecular indicator expressly designed to quantify the local environment of each molecule. More precisely, Ψ_i is defined as the minimum

distance in real space between all pairs $i-j$, where the index j runs over all molecules at a chemical distance of four from i . Once a proper definition of H-bond is accepted, this new indicator Ψ_i does not require any arbitrary cut-off in its definition, eliminating the possibility of cut-off dependent findings. In Ref. 44, it was shown that averaging Ψ_i over all molecules in the system produces a global (as opposed to local) indicator that accurately describes the critical fluctuations in the vicinity of the liquid–liquid critical point, which, for the TIP4P/Ice model, was estimated at $T_c \approx 188.6$ K, $P_c \approx 1750$ bars, and $\rho_c \approx 1.015$ g/cm³.¹⁷

Figure 1 shows the distribution of Ψ_i for different pressures at deep supercooled conditions, below ($T = 188$ K) and above ($T = 190$ K) the critical temperature $T_c \approx 188.6$ K.¹⁷ To subtract the trivial isotropic scaling component from the relative distances by varying the density, we show the distribution as a function of $\Psi^* \equiv \Psi[\frac{\rho(T,P)}{1 \text{ g/cm}^3}]^{1/3}$, where $\rho(T,P)$ is the temperature and pressure dependent density. At low pressures ($P < 1000$ bars), the distribution is asymmetric and centered around $\Psi^* \approx 0.6$ nm, with a negligible tail below $\Psi^* \approx 0.4$ nm. With increasing pressure, this last region starts to be populated. Below T_c , the distribution jumps from the low density to the high density liquid value, while the same change is observed progressively at temperatures above (but close to) T_c . The crossover from the open tetrahedral distance $\Psi^* \approx 0.6$ nm to the interstitial distance $\Psi^* \approx 0.35$ nm is clearly detectable from the distribution functions. In addition to the crossover, the distributions show a marked two-peak behavior, with an approximate crossing (isosbestic) point around $\Psi^* \approx 0.5$ nm. The clear two-peak structure provides indisputable evidence of two major local environments characterizing supercooled water, significantly reinforcing the underlying idea on which two-state models have been developed in

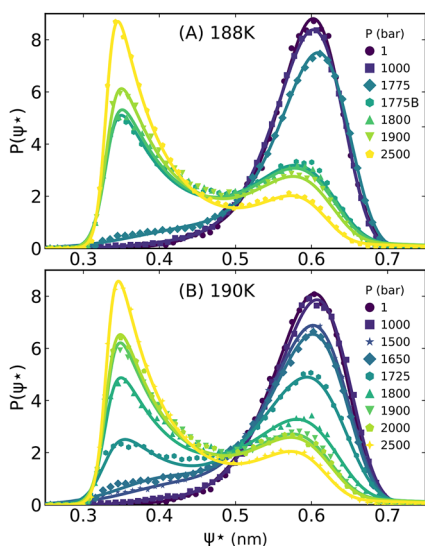


FIG. 1. Pressure dependence of the Ψ^* distribution along (a) a sub-critical isotherm $T = 188$ K and (b) a super-critical isotherm $T = 190$ K. A clear bimodal behavior is manifested. The simulation labeled 1775B was initialized from a high-density configuration as opposed to the one labeled 1775 bars, which was initialized from a low-density configuration. The points represent simulation data, and the solid lines represent the regression from Eq. (1).

the past. Data in Fig. 1 also show that, as expected, the two coexisting liquids (data for $P = 1775$ bars at $T = 188$ K) are not “pure,” the low-density liquid containing a small fraction of interstitial molecules and, vice versa, the high-density liquid containing a non-negligible fraction of tetrahedral local structures.

To highlight the temperature dependence, we next consider the behavior of Ψ^* along four different isobars (1, 1000, 1700, and 2500 bars) from 300 K down to T_c . The two lowest isobars are characterized by a significant change in density upon cooling. Figure 2 shows that the change in density is accompanied by a significant change in the structure of the liquid, as revealed by the distributions of Ψ^* . Both for $P = 1$ and $P = 1000$ bars, the fraction of interstitial molecules decreases on cooling, almost vanishing at the lowest temperature, consistent with the expectation that interstitial local configurations are characterized by a higher energy per molecule. The density change with temperature at $P = 1700$ and $P = 2500$ bars is significantly more limited, and correspondingly, the Ψ^* distributions do not show a significant change. At all state points, the two-peak structure is very evident, confirming that the two families of local environments are already very well characterized at ambient temperatures. We stress that above the critical point, there is a single free energy minimum in supercritical conditions, which encompasses two structurally distinct families. At the single molecule level, the two families unequivocally exist, as shown by the bimodality of $P(\Psi)$.

The data in Fig. 2 show that a pure tetrahedral system is reached at very deep supercooling at ambient pressure. The opposite limit, in which essentially all molecules have interstitial neighbors, is found in the very-high density limit, again at low temperatures. To show this, we follow at $T = 188$ K the evolution of the distribution of Ψ with pressure in the region between 2000 and 13 000 bars, where the high density liquid continuously transforms into a very high density structure. This process, described in Fig. 3, is accompanied by the progressive disappearance of molecules with large Ψ . Around 13 000 bars, all molecules have at least one interstitial neighbor, and $P(\Psi^*)$ peaks around 0.35 nm.

We also observe that Ψ , unlike other indicators, is not critically affected by being evaluated using the inherent structure coordinates. When evaluated in real dynamics (i.e., the structures directly sampled during the simulation before the suppression of thermal vibrations via energy minimization), the features of Ψ at low T are fundamentally unchanged (see Fig. 4). The peaks trivially display a slight broadening due to the vibrational noise (and, hence, also a relatively less accurate definition of H-bond), but the shape of the distribution, its bimodality, and the large separation between the two configurations are all well-conserved properties, highlighting the robustness of the structural description provided by Ψ . The agreement between RD and IS apparently deteriorates with increasing T (Fig. 5). The differences arise from the misidentification of H-bonds in the RD configurations at higher temperatures (needed to define the topological distances used to compute Ψ). Indeed, as discussed in detail in the supplementary material, at higher temperatures, the distribution of molecular distances and orientations is widened by the increasing contribution of vibrational and librational modes, mixing the configurations corresponding to H-bonded and non-H-bonded pairs. Above ≈ 240 K, the two distributions (bonded and non-bonded, see Fig. S3) are so widened by thermal motion that they superimpose in the region where the Luzar–Chandler cutoff

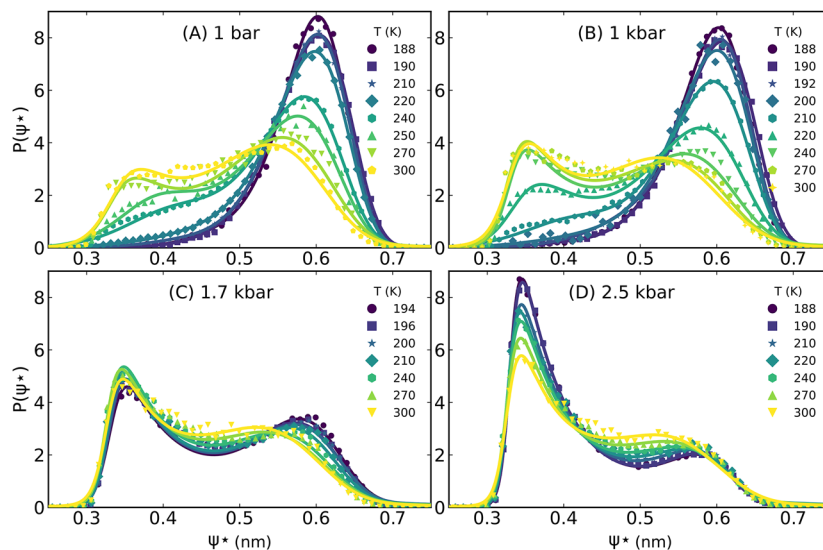


FIG. 2. Temperature dependence of $P(\Psi^*)$ for four different pressure values. The points represent simulation data, and the solid lines represent the regression from Eq. (1).

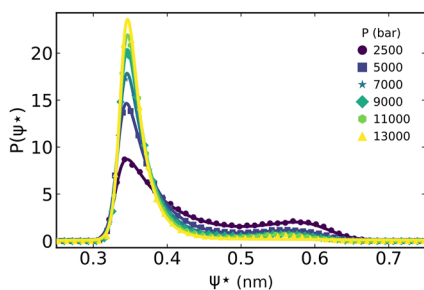


FIG. 3. Crossover from the high-density liquid to the very high-density structure as reflected by the $P(\Psi^*)$ distribution at $T = 188$ K. In a continuous way, all molecules become surrounded by interstitial molecules. The points represent simulation data, and the solid lines represent the regression from Eq. (1).

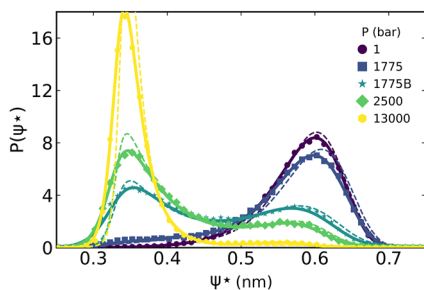


FIG. 4. Distribution of Ψ^* evaluated in the real dynamics conserves the bimodality and the wide separation of the two local states that are observed in the inherent structures. Shown here selected points along the $T = 188$ K isotherm. The thin dashed lines represent the distributions at the corresponding thermodynamic states in the inherent structures.

acts. However, if the distribution of Ψ is evaluated using the spatial configuration of the RD while retaining the H-bond network identified in the corresponding IS configuration (thick violet curves in Fig. 5), then the same agreement between RD and IS that was observed at $T = 188$ K is found at all temperatures.

At all the conditions we analyzed, the Ψ^* distributions can be faithfully represented as a mixture of two Burr type XII distributions,⁵¹

$$P(\Psi) = sP_L(\Psi; c_L, k_L, \lambda_L) + (1 - s)P_H(\Psi; c_H, k_H, \lambda_H), \quad (1)$$

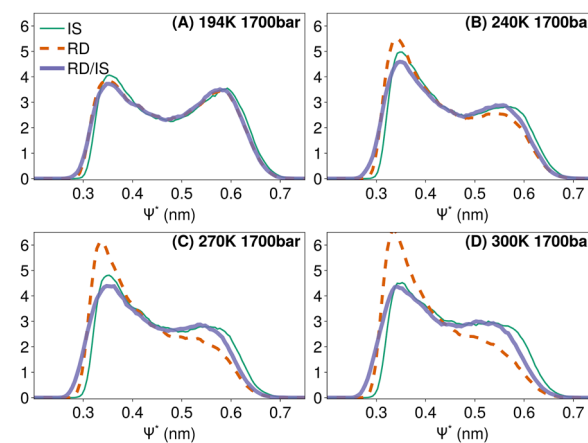


FIG. 5. Distribution of Ψ^* evaluated from 194 to 300 K along the 1700 bars isobar shows no significant differences between inherent structures and real dynamics, provided that H-bonds are properly identified. Curves labeled "IS" and "RD" (thin green and dashed orange, respectively) correspond to Ψ^* distributions evaluated in the inherent structures and real dynamics. Curves labeled "RD/IS," in thick violet, have been evaluated using the spatial configuration of the RD but employing the definition of the H-bond network obtained from the IS.

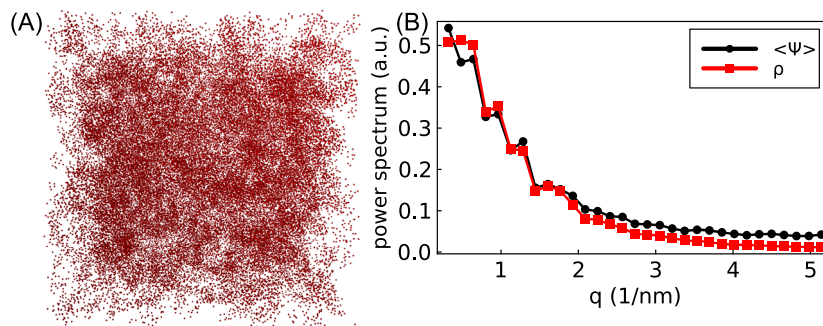


FIG. 6. (a) Snapshot of molecules with low Ψ^* from a constant-density simulation with 250 000 molecules at $T = 191$ K and $\rho = 1.015$ g/cm³ visually shows spatial correlations extending over large length-scales. (b) Comparison between the power spectrum of the averaged Ψ^* field (multiplied along y by an arbitrary factor) and the power spectrum of the density field ρ (i.e., the structure factor), evaluated in the IS configurations, confirms that these two scalar fields show the same spatial correlations. The same calculation was also performed in the RD configurations (Fig. S6) and shows no noticeable difference from the calculations in the IS.

whose parameters (c, k, λ) and relative weights (s) were optimized independently for each thermodynamic condition. These fits are superimposed as solid lines on the simulation data in Figs. 1–4. The behavior of the distribution parameters (see the supplementary material) suggests that a non-trivial dependence on thermodynamic conditions is still present after removing the isotropic scaling component, preventing us from obtaining a simpler description of the behavior of Ψ^* .

To provide a graphical representation of the spatial correlation of the molecules with similar Ψ values, we perform and analyze a simulation of a 250 000 molecule system at $T = 190$ K and $\rho = 1.015$ g/cm³, corresponding to the critical isochore of the TIP4P/Ice model. The 250 000 molecule system is contained in a cubic box of about 19.5 nm. Such a large distance—more than 60 times the nearest neighbor oxygen–oxygen distance (0.28 nm)—makes it possible to investigate the presence of long range correlations. Figure 6(a) shows, with a red sphere, the position of the molecules with $\Psi^* < 0.45$ nm. Eyes immediately catch the spatial correlation between them, with a correlation scale significantly larger than the nearest neighbor distance. Such a correlation is a clear indication of a net attraction between molecules in similar environments. This observation can be quantified and strengthened by calculating the structure factor and the power spectrum of the Fourier transform of the density, shown in Fig. 6(b) (evaluated in the IS configurations). As expected close to the critical point, and as previously demonstrated for the ST2 water model⁵³ and also for TIP4P/2005 and TIP4P/Ice in smaller-sized systems,¹⁷ a strong increase in the scattered intensity at small q is observed. To provide evidence that this correlation is brought up by the correlation between molecules in similar environments, we define a $\langle \Psi \rangle$ field by averaging Ψ_i over all molecules included in a small cubic volume. For convenience, we pick this volume as $(L/32)^3$, where L is the simulation box side. With this choice, there are about eight molecules in each mesh volume. The resulting field $\langle \Psi \rangle$ can then be Fourier transformed in space and its power spectrum compared with $S(q)$. The result of this comparison is shown in Fig. 6(b), which, by the similarity of the two Fourier transforms, neatly demonstrates that the density field and the $\langle \Psi \rangle$ field not only provide the same information but also that the spatial correlation in the density picked up by the small-angle scattering is identical to the spatial correlation of

$\langle \Psi \rangle$. In this respect, the two families of molecules can be identified as the two states commonly assumed in mean field models.

IV. CONCLUSIONS

In this article, we have demonstrated that two distinct families of local environments can be clearly identified in numerical simulations of bulk liquid water on the basis of the structural indicator Ψ_i . This indicator quantifies the distance from a central molecule i to the closest molecule separated by four hydrogen bonds. In this respect, it requires information on the connectivity and local geometry of the hydrogen bond network departing from each molecule. The distribution of Ψ_i becomes unimodal in two extreme cases, both at deep supercooling: at $T = 188$ K, below the critical pressure and at ambient pressure, all molecules belong to the large Ψ family, while at $T = 188$ K and pressures above 10 kbar (when the configuration of water in the supercooled liquid is reminiscent of the very-high density amorphous structure⁴³), all molecules belong to the small Ψ family. Since the small Ψ family is characterized by the presence of interstitial molecules between the first and second tetrahedral shells, the very high density amorphous structure can be described as the limiting structure in which, despite the hydrogen bonds being mostly preserved (with only $\sim 10\%$ of the molecules showing coordination defects at 13 kbar⁴³), all molecules are surrounded by and act as interstitial molecules. The bimodal character of Ψ is also conserved at ambient conditions, where, despite the increased thermal noise leading to a broadening of the two peaks and the existence of a single free energy minimum (at the system level), it is still possible to clearly discern two structural families (at the single molecule level, in terms of Ψ).

The present findings provide strong support for theoretical modeling of the thermodynamics of water as arising from the relative competition between these two families of local environments, each of which is characterized by its own local energy, density, and entropy. The water anomalies originate from the competition between these two local structures, a phenomenon that is missing in simple liquids.

Finally, we have demonstrated that these local structures cluster in space. The analysis of a very large simulation, with more than

250 000 molecules and providing access to distances extending up to 10 nm, allows us to demonstrate that the correlation goes well beyond the 0.8–1 nm range, which has long been associated with the typical decay of the spatial correlations in water,⁵⁴ thus confirming the preferential association of molecules of similar type, a feature that is essential for the existence of the liquid–liquid critical phenomenon.

SUPPLEMENTARY MATERIAL

The supplementary material includes data on the phase diagram of the TIP4P/Ice model of water used in the present work, a discussion on the identification of hydrogen bonds, additional data relative to the parameterization of the Ψ^* distribution through Burr type XII distributions, and the comparison between inherent structures and real dynamics.

ACKNOWLEDGMENTS

F.S. acknowledges support from PRIN 2022JWAF7Y, ICSC—Centro Nazionale di Ricerca in High Performance Computing, Big Data, and Quantum Computing, funded by the European Union—NextGenerationEU, and CINECA-ISCRA.

AUTHOR DECLARATIONS

Conflict of Interest

The authors have no conflicts to disclose.

Author Contributions

Riccardo Foffi: Formal analysis (equal); Writing – review & editing (equal). **Francesco Sciortino:** Data curation (equal); Formal analysis (equal); Writing – original draft (equal); Writing – review & editing (equal).

DATA AVAILABILITY

The data that support the findings of this study are available within the article. Additional data (MD trajectories) are available from the corresponding author upon reasonable request.

REFERENCES

- ¹P. G. Debenedetti, *J. Phys.: Condens. Matter* **15**, R1669 (2003).
- ²P. Gallo, K. Amann-Winkel, C. A. Angell, M. A. Anisimov, F. Caupin, C. Chakravarty, E. Lascaris, T. Loerting, A. Z. Panagiotopoulos, J. Russo, J. A. Sellberg, H. E. Stanley, H. Tanaka, C. Vega, L. Xu, and L. G. M. Pettersson, *Chem. Rev.* **116**, 7463 (2016).
- ³P. H. Handle, T. Loerting, and F. Sciortino, *Proc. Natl. Acad. Sci. U. S. A.* **114**, 13336 (2017).
- ⁴H. Tanaka, *J. Chem. Phys.* **153**, 130901 (2020).
- ⁵K. H. Kim, A. Späh, H. Pathak, F. Perakis, D. Mariedahl, K. Amann-Winkel, J. A. Sellberg, J. H. Lee, S. Kim, J. Park, K. H. Nam, T. Katayama, and A. Nilsson, *Science* **358**, 1589 (2017).
- ⁶J. Russo, F. Leoni, F. Martelli, and F. Sciortino, *Rep. Prog. Phys.* **85**, 016601 (2022).

- ⁷F. Smullenburg and F. Sciortino, *Phys. Rev. Lett.* **115**, 015701 (2015).
- ⁸A. K. Soper and M. A. Ricci, *Phys. Rev. Lett.* **84**, 2881 (2000).
- ⁹L. B. Skinner, M. Galib, J. L. Fulton, C. J. Mundy, J. B. Parise, V.-T. Pham, G. K. Schenter, and C. J. Benmore, *J. Chem. Phys.* **144**, 134504 (2016).
- ¹⁰H. Tanaka, *J. Chem. Phys.* **112**, 799 (2000).
- ¹¹V. Holten and M. A. Anisimov, *Sci. Rep.* **2**, 713 (2012).
- ¹²J. W. Biddle, R. S. Singh, E. M. Sparano, F. Ricci, M. A. González, C. Valeriani, J. L. F. Abascal, P. G. Debenedetti, M. A. Anisimov, and F. Caupin, *J. Chem. Phys.* **146**, 034502 (2017).
- ¹³J. Niskanen, M. Fondell, C. J. Sahle, S. Eckert, R. M. Jay, K. Gilmore, A. Pietzsch, M. Dantz, X. Lu, D. E. McNally, T. Schmitt, V. Vaz Da Cruz, V. Kimberg, F. Gel'mukhanov, and A. Föhlisch, *Proc. Natl. Acad. Sci. U. S. A.* **116**, 4058 (2019).
- ¹⁴A. K. Soper, *J. Chem. Phys.* **150**, 234503 (2019).
- ¹⁵G. P. Johari and J. Teixeira, *J. Phys. Chem. B* **119**, 14210 (2015).
- ¹⁶P. H. Poole, F. Sciortino, U. Essmann, and H. E. Stanley, *Nature* **360**, 324 (1992).
- ¹⁷P. G. Debenedetti, F. Sciortino, and G. H. Zerze, *Science* **369**, 289 (2020).
- ¹⁸J. Weis, F. Sciortino, A. Z. Panagiotopoulos, and P. G. Debenedetti, *J. Chem. Phys.* **157**, 024502 (2022).
- ¹⁹T. E. Gartner, L. Zhang, P. M. Piaggi, R. Car, A. Z. Panagiotopoulos, and P. G. Debenedetti, *Proc. Natl. Acad. Sci. U. S. A.* **2020**, 15440.
- ²⁰A. Eltareb, G. E. Lopez, and N. Giovambattista, *Sci. Rep.* **12**, 6004 (2022).
- ²¹O. Mishima and H. E. Stanley, *Nature* **392**, 164 (1998).
- ²²K. Winkel, E. Mayer, and T. Loerting, *J. Phys. Chem. B* **115**, 14141 (2011).
- ²³K. H. Kim, K. Amann-Winkel, N. Giovambattista, A. Späh, F. Perakis, H. Pathak, M. L. Parada, C. Yang, D. Mariedahl, T. Eklund, T. J. Lane, S. You, S. Jeong, M. Weston, J. H. Lee, I. Eom, M. Kim, J. Park, S. H. Chun, P. H. Poole, and A. Nilsson, *Science* **370**, 978 (2020).
- ²⁴K. Amann-Winkel, K. H. Kim, N. Giovambattista, M. Ladd-Parada, A. Späh, F. Perakis, H. Pathak, C. Yang, T. Eklund, T. J. Lane, S. You, S. Jeong, J. H. Lee, I. Eom, M. Kim, J. Park, S. H. Chun, P. H. Poole, and A. Nilsson, *Nat. Commun.* **14**, 442 (2023).
- ²⁵M. J. Cuthbertson and P. H. Poole, *Phys. Rev. Lett.* **106**, 115706 (2011).
- ²⁶Y. Li, J. Li, and F. Wang, *Proc. Natl. Acad. Sci. U. S. A.* **110**, 12209 (2013).
- ²⁷R. S. Singh, J. W. Biddle, P. G. Debenedetti, and M. A. Anisimov, *J. Chem. Phys.* **144**, 144504 (2016).
- ²⁸F. Caupin and M. A. Anisimov, *Phys. Rev. Lett.* **127**, 185701 (2021).
- ²⁹Z. Yu, R. Shi, and H. Tanaka, *J. Phys. Chem. B* **127**, 3452 (2023).
- ³⁰M. A. Anisimov, M. Duška, F. Caupin, L. E. Amrhein, A. Rosenbaum, and R. J. Sadus, *Phys. Rev. X* **8**, 011004 (2018).
- ³¹J. R. Errington and P. G. Debenedetti, *Nature* **409**, 318 (2001).
- ³²E. Shiratani and M. Sasai, *J. Chem. Phys.* **104**, 7671 (1996).
- ³³J. Russo and H. Tanaka, *Nat. Commun.* **5**, 3556 (2014).
- ³⁴H. Tanaka, H. Tong, R. Shi, and J. Russo, *Nat. Rev. Phys.* **1**, 333 (2019).
- ³⁵J. M. Montes de Oca, F. Sciortino, and G. A. Appignanesi, *J. Chem. Phys.* **152**, 244503 (2020).
- ³⁶A. R. Verde, J. M. M. de Oca, S. R. Accordino, L. M. Alarcón, and G. A. Appignanesi, *Eur. Phys. J. E* **44**, 47 (2021).
- ³⁷A. V. Muthachikavil, G. M. Kontogeorgis, X. Liang, Q. Lei, and B. Peng, *Phys. Rev. E* **105**, 034604 (2022).
- ³⁸C. Faccio, M. Benzi, L. Zanetti-Polzi, and I. Daidone, *J. Mol. Liq.* **355**, 118922 (2022).
- ³⁹A. Neophytou, D. Chakrabarti, and F. Sciortino, *Nat. Phys.* **18**, 1248 (2022).
- ⁴⁰N. A. Loubet, A. R. Verde, J. A. Lockhart, and G. A. Appignanesi, *J. Chem. Phys.* **159**, 064512 (2023).
- ⁴¹I. Daidone, R. Foffi, A. Amadei, and L. Zanetti-Polzi, *J. Chem. Phys.* **159**, 094502 (2023).
- ⁴²R. Foffi, J. Russo, and F. Sciortino, *J. Chem. Phys.* **154**, 184506 (2021).
- ⁴³R. Foffi and F. Sciortino, *Phys. Rev. Lett.* **127**, 175502 (2021).
- ⁴⁴R. Foffi and F. Sciortino, *J. Phys. Chem. B* **127**, 378 (2023).
- ⁴⁵M. J. Abraham, T. Murtola, R. Schulz, S. Páll, J. C. Smith, B. Hess, and E. Lindahl, *SoftwareX* **1–2**, 19 (2015).
- ⁴⁶J. L. F. Abascal, E. Sanz, R. García Fernández, and C. Vega, *J. Chem. Phys.* **122**, 234511 (2005).
- ⁴⁷F. Sciortino, *J. Stat. Mech.* **2005**, P05015.

⁴⁸L. Lupi, B. Vázquez Ramírez, and P. Gallo, *J. Chem. Phys.* **155**, 054502 (2021).

⁴⁹J. R. Espinosa, J. L. F. Abascal, L. F. Sedano, E. Sanz, and C. Vega, *J. Chem. Phys.* **158**, 204505 (2023).

⁵⁰A. Luzar and D. Chandler, *J. Chem. Phys.* **98**, 8160 (1993).

⁵¹I. W. Burr, *Ann. Math. Stat.* **13**, 215 (1942).

⁵²D. Mariedahl, F. Perakis, A. Späh, H. Pathak, K. H. Kim, G. Camisasca, D. Schlesinger, C. Benmore, L. G. M. Pettersson, A. Nilsson, and K. Amann-Winkel, *J. Phys. Chem. B* **122**, 7616 (2018).

⁵³J. Guo, R. S. Singh, and J. C. Palmer, *Mol. Phys.* **116**, 1953 (2018).

⁵⁴F. Sciortino and S. L. Fornili, *J. Chem. Phys.* **90**, 2786 (1989).